



Size variation and magnetic dilution effects on the structure and magnetic properties of cobalt zinc ferrite

L. R. Gonsalves^{1,2}, S. G. Gawas^{2,3}, Sher Singh Meena⁴, and V. M. S. Verenkar^{2,*}

¹Department of Chemistry, Parvatibai Chowgule College of Arts and Science, Margao, Goa 403602, India

²School of Chemical Sciences, Goa University, Taleigao, Goa 403206, India

³Department of Chemistry, Dnyanprassarak Mandal's College and Research Centre, Assagao, Mapusa, Goa 403507, India

⁴Solid State Physics Division, Bhabha Atomic Research Centre, Mumbai 400085, India

Received: 24 March 2022

Accepted: 24 July 2022

Published online:

19 August 2022

© The Author(s), under exclusive licence to Springer Science+Business Media, LLC, part of Springer Nature 2022

ABSTRACT

Nanocrystalline cobalt zinc ferrites $\text{Co}_{1-x}\text{Zn}_x\text{Fe}_2\text{O}_4$ ($x = 0.0, 0.2, 0.4, 0.5, 0.6, 0.8, 1.0$), have been prepared by employing a precursor combustion method via decomposition of the metal carboxylato hydrazinate precursors. This synthesis technique yields nanoparticles with particle size between 12 and 15 nm as determined from transmission electron microscopy (TEM) studies. The nanoferrites were then sintered at 1000 °C for 15 h to obtain micrometer size 'bulk' ferrites in the range of 0.3–0.8 μm . X-ray diffraction (XRD) and Fourier transform infrared (FTIR) Spectroscopy confirmed the formation of the mixed ferrites without any impurities. Addition of non-magnetic ion like Zn^{2+} into the crystal structure of cobalt ferrite leads to a prominent change in the size, structure and properties. The saturation magnetization values (M_S) increases upto $x = 0.4$ and then decreases with further increase in Zn concentration. A maximum M_S value of 90.85 emu/g and 79.59 emu/g for $x = 0.4$ was obtained for the sintered and nanoferrite sample, respectively. The lower M_S and higher coercivity (H_C) values for nanoferrites than the sintered ferrites exhibited a strong dependence on the particle size due to the cation distribution and surface effects. The Curie temperature (T_C) was found to decrease appreciably with the reduction in particle size and with increasing concentration of Zn. The room temperature Mössbauer spectra showed a transition from ferrimagnetic to a paramagnetic state with increasing zinc concentration along with superparamagnetic features which was in corroboration with VSM studies.

Address correspondence to E-mail: vmsv@rediffmail.com

1 Introduction

Magnetic materials are indispensable in this age of technology, for a myriad of applications ranging from electronics to medicine. Among the various magnetic materials known today, the magnetic spinel ferrites have emerged as versatile materials for use in numerous technological and biological applications, such as drug delivery, magnetic resonance imaging (MRI), catalysis, gas sensing. [1–5]. There is a renewed interest in these oldest materials in the nanomaterial form due to its unusual magnetic properties which are not observed in the bulk material. As the dimensions are reduced to a nanoscale the magnetic properties are known to change significantly. For example, reduction in saturation magnetisation, shift in Curie temperature, single domain nature, etc. [6–8]. Superparamagnetism, another unique feature exhibited by the magnetic nanoparticles, coupled with tuneable surface properties, makes them valuable as contrast agents for MRI [4]. Cobalt ferrite, a magnetic spinel, has received considerable attention owing to its useful magnetic properties, which can be tailored for specific application [9–11]. The magnetic properties of cobalt ferrite (CoFe_2O_4) can be suitably controlled by substituting the cation Co^{2+} with a non-magnetic ion like Zn^{2+} giving rise to homogenous solid solutions of mixed ferrites ($\text{Co}_{1-x}\text{Zn}_x\text{Fe}_2\text{O}_4$) [12–15]. The cobalt ferrite is an inverse spinel while the zinc ferrite is a normal one. However, the mixed compositions are either random or may vary from normal to inverse depending on the distribution of the cations at the tetrahedral and octahedral sites. Although the site occupancy can be determined quite accurately for simple ferrites, the task is quite challenging for mixed ferrite compositions. The distribution of the metal ions in the two sites depends on factors such as, the electrostatic energy due to repulsion and attraction between the anions and cations, Crystal field stabilization energy (CFSE), magnetic ordering energy, etc. The site preference for individual cation is generally expressed in terms of particular site stabilization energy [16]. Moreover, reducing the size to nano dimensions will cause spatial confinement and related effects like large surface to volume ratio, surface anisotropy, and spin disorder that will determine the overall distribution of cations and the resultant properties [7].

The magnetic properties of ferrite nanoparticles depend on the size of particles not only directly, but

also indirectly, through the influence of the small size on the structure of nanoparticles. It is known that the structure of nanoparticles is more flexible as compared to the 'bulk' structure. Usually, it adapts to the small size and the large surface-to-volume ratio resulting in distribution of atoms over different lattice sites that is significantly different to that of the bulk material. The deviations in the nanocrystal structure from the ideal 'bulk' state have been studied by many researchers [17–19]. The flexibility in the nanoparticles crystal structure allows for large compositional deviations from the bulk stoichiometry without losing the single-phase structure. Also, below a critical grain size the domain structure of the particles changes from multidomain to single domain behavior resulting in interesting magnetic properties. Magnetic domains are known to exist in Ferro- or Ferri-magnetic materials. Essentially, most of the phenomena associated with magnetic properties such as coercivity, saturation magnetisation, magnetoresistance, Curie temperature, etc. are closely related to domains [20, 21]. Literature reveals that, the properties of a material are largely influenced by size and shape conditions which in turn depend on the method of synthesis. The effect of size on the properties is paramount for all application purposes. Available reports focus mainly on the size-property relationship of either the bulk or nanosize cobalt zinc ferrite for a few compositions. A systematic study on the variation of size and its influence on the resultant properties were found to be lacking.

In the present work, the primary aim was to investigate the effect of grain size on the structural and magnetic properties of cobalt zinc ferrites. Additionally, we also aimed to study the effect of magnetic dilution on the resultant properties of the bulk and nanoferrites by substituting cobalt with a non-magnetic atom like Zn. Varying concentration of Zn has been substituted in the cobalt ferrite to ascertain the controllability of the magnetic properties of cobalt ferrite. With this objective, the Curie temperature (T_C), domain nature of the samples along with the superparamagnetic behavior of the nanoparticles and its size-dependency has been determined. The studies presented here aid in understanding the behavior of the nanosized ferrites in comparison with its submicron size 'bulk' counterparts thus illustrating size effects on the measured properties.

2 Experimental

2.1 Materials and methods

The method of synthesis governs the size and ultimately the properties of the material which has almost become a thumb rule for material chemists. Literature is replete with synthesis techniques for preparing nanosized ferrites. Synthesis of cobalt zinc ferrite $\text{Co}_{1-x}\text{Zn}_x\text{Fe}_2\text{O}_4$ ($x = 0.0$ to 1.0) nanoparticles have been carried out by a precursor combustion technique which has been reported by our group [22]. All the chemicals used were of analytical grade without further purification. A requisite quantity of sodium fumarate in aqueous medium was stirred with hydrazine hydrate $\text{N}_2\text{H}_4\cdot\text{H}_2\text{O}$ (99–100%) in the atmosphere of nitrogen gas as an inert medium for 2 h. To this solution, a stoichiometric amount of freshly prepared ferrous chloride solution mixed with cobalt chloride and zinc chloride was added drop wise with constant stirring in an inert nitrogen atmosphere. The precursor thus obtained was filtered, washed with ethanol and dried with diethyl ether. This dried precursor was then auto catalytically decomposed to yield nanosized ferrite. The ferrite powder was heated at $400\text{ }^\circ\text{C}$ for 2 h to remove any traces of residual carbon. The samples so obtained were termed ‘as prepared’ ferrites. This ‘as prepared’ ferrite powder was pelletized and pre-sintered at $800\text{ }^\circ\text{C}$ for 5 h, the pellets were then crushed and ground using agate mortar and pestle and again pressed into pellets of 1 cm diameter and 0.2 cm thickness and later subjected to final sintering at $1000\text{ }^\circ\text{C}$ for 15 h to obtain the bulk samples.

2.2 Characterization

The phase purity and the crystal structure for all ‘as prepared’ and sintered cobalt zinc ferrite samples were investigated using X-ray diffraction (XRD) technique on a RIGAKU ULTIMA IV X-ray diffractometer using Cu-K_α radiations of wavelength 1.5418 \AA (filtered through Ni). The Fourier transform-infrared (FTIR) spectra of the samples reported here are recorded on a Shimadzu IR prestige 21 spectrometer at ambient conditions. The sample powder was mixed with KBr in the ratio of 1:10 and the scanning range selected was from 4000 to 300 cm^{-1} . The spectra were recorded in the diffuse reflectance mode. The morphology of ‘as prepared’ and sintered

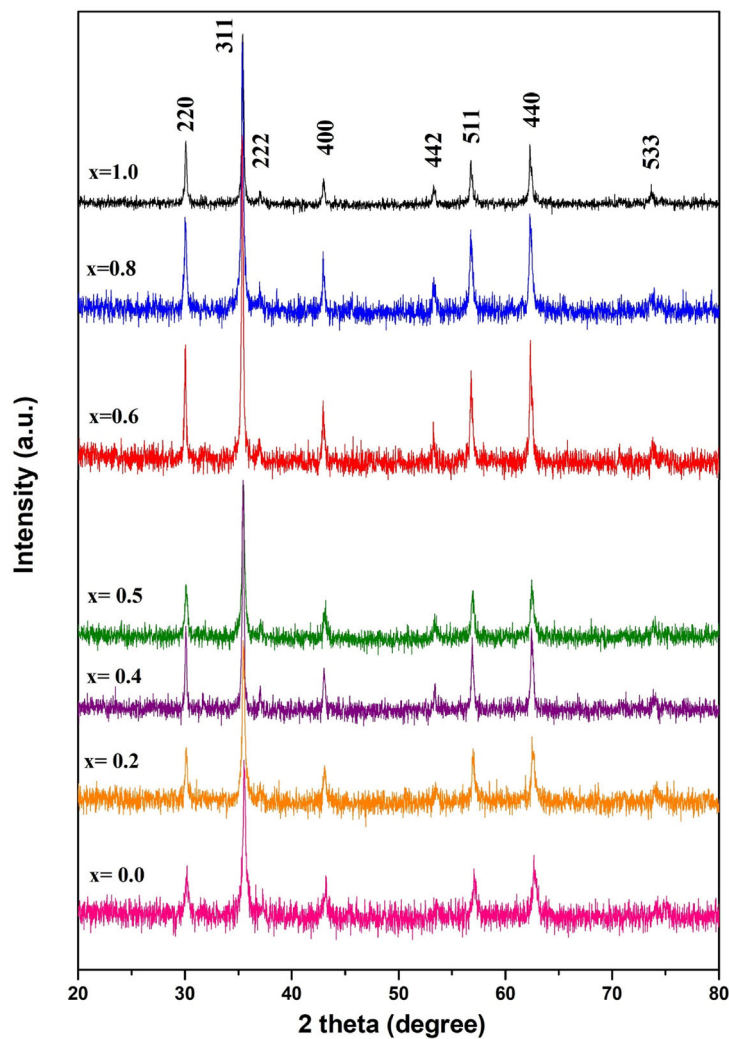
samples was observed by transmission electron microscopy (TEM) using a JEM 2000 CX electron microscope and scanning electron microscopy (SEM) using a JEOL-JSM 6390 LV electron microscope respectively. The surface area of the ferrite compositions were measured using Brunauer–Emmett–Teller (BET) surface area analyzer SMART SORB 90/91 at liquid nitrogen temperature. The domain nature of the particles and the Curie temperature was determined using a temperature programmable AC magnetic susceptibility system. The magnetic measurements were carried out on a Vibrating Sample Magnetometer (VSM, Quantum Design VersaLab). Mössbauer spectroscopy was employed to study the cation distribution as well as the magnetic behavior of the nanosized and bulk ferrites. Mössbauer spectra at room temperature were recorded using a Mössbauer spectrometer, operated in constant acceleration mode (triangular wave) in transmission geometry. The source employed was Co-57 in Rh matrix of strength 50 mCi . The calibration of the velocity scale was done using an enriched $\alpha\text{-}^{57}\text{Fe}$ metal foil using a value of 331 kOe for the effective nuclear hyperfine field (H_{eff}) at room temperature. The outer line width of calibration spectra is 0.29 mm/s . The Mössbauer spectra were fitted using WinNormos fit programme with Lorentzian distribution. The results of isomer shift are relative to $\alpha\text{-Fe}$ metal foil ($\delta = 0.00\text{ mm/s}$).

3 Results and discussion

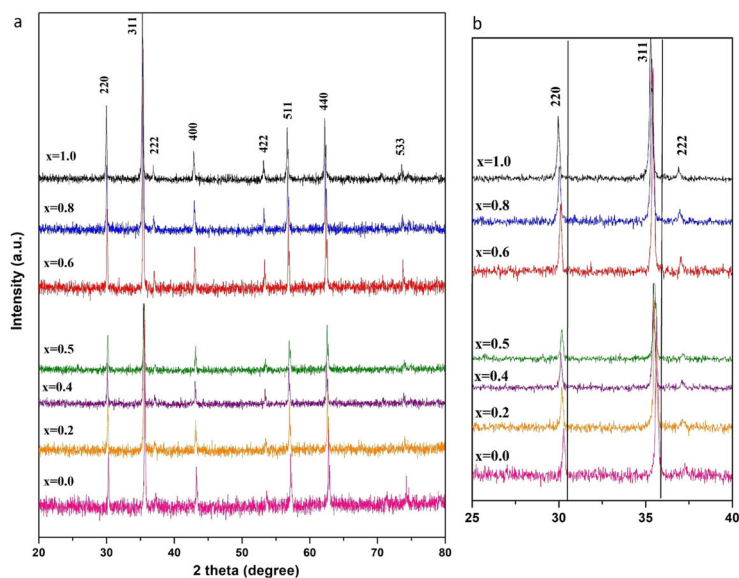
3.1 X-ray diffraction (XRD) analysis

The mixed cobalt zinc ferrite, $\text{Co}_{1-x}\text{Zn}_x\text{Fe}_2\text{O}_4$, ($x = 0.0\text{--}1.0$) have been investigated by X-ray diffraction technique between 20° and 80° to check its phase purity and crystallinity. The XRD patterns of the ‘as prepared’ and sintered samples are shown in Fig. 1a and b, respectively. All the compositions of Co–Zn ferrite samples could be indexed in terms of a single phase cubic spinel structure using the standard ICDD card # 01-1121 for CoFe_2O_4 . It can be seen from Fig. 1a that the ‘as prepared’ samples show peak broadening indicative of nanosized particles with large surface/volume ratio whereas sintering brings about grain growth leading to crystallinity and sharp peaks in the case of bulk samples in Fig. 1b. A slight shift in peak positions is also noted with the increase

Fig. 1 a X-ray diffraction pattern of ‘as prepared’ $\text{Co}_{1-x}\text{Zn}_x\text{Fe}_2\text{O}_4$ ($x = 0.0-1.0$). **b** X-Ray Diffraction pattern of ‘sintered’ $\text{Co}_{1-x}\text{Zn}_x\text{Fe}_2\text{O}_4$ ($x = 0.0-1.0$)



a X-Ray Diffraction pattern of ‘as prepared’ $\text{Co}_{1-x}\text{Zn}_x\text{Fe}_2\text{O}_4$ ($x=0.0-1.0$).



b X-Ray Diffraction pattern of ‘sintered’ $\text{Co}_{1-x}\text{Zn}_x\text{Fe}_2\text{O}_4$ ($x=0.0-1.0$).

in Zn content. Using the XRD data, we investigated the role of the Zn-substitution in modifying the structural parameters such as the lattice constant (a), ionic radii (r_A and r_B), the distance between the magnetic ions (L_A and L_B) and bond lengths (A–O and B–O) of tetrahedral (A) sites and octahedral (B) sites in cubic spinel structure of the nanosized and bulk cobalt zinc ferrite. The values of various structural parameters are given in Table 1. An increase in the lattice constant a , calculated using d value and related hkl (311) value, is observed with increase in Zn concentration almost in a linear manner, thus obeying Vegard's law [14, 15] which indicates the formation of homogenous solutions of cobalt zinc ferrite. The increase in a is due to the substitution of smaller ion of Co^{2+} having ionic radii of 0.72 Å by bigger Zn^{2+} with ionic radii of 0.74 Å [14]. Furthermore, the lattice constant of nanoferrites is found to be slightly less than that of its bulk counterparts. This decrease cannot be explained on the basis of cation rearrangement in the spinel lattice only but may also be due to particle size effect, more specifically, the effect of surface stress. The surface stress causes small particles to be in a state of compression where the internal pressure is inversely proportional to the radius of the particle [23]. Thus, the surface lattice contraction is clearly felt for the nanosized ferrites whereas for the bulk samples, sintering at high temperature leads to greater degree of lattice ordering. Nanosized cobalt zinc ferrites having lower lattice constants than the bulk compounds have been reported by Veverka et al. [24]. The cation distribution in the case of mixed ferrites is difficult to

estimate accurately. However, an attempt has been made to calculate theoretically the hopping lengths in the tetrahedral (L_A) and octahedral (L_B) site, ionic radii at tetrahedral (r_A) and octahedral (r_B) site and the tetrahedral (A–O) and octahedral (B–O) bond lengths. The calculations were done using equations reported in literature [14, 15] which are based on the lattice constant a obtained from the XRD data. The mean ionic radius of the tetrahedral (A) site " r_A " and octahedral (B) site, " r_B " has been calculated using the following relation;

$$r_A = a\sqrt{3}(u - 0.25) - R_o \quad (1)$$

$$r_B = a(5/8 - u) - R_o \quad (2)$$

where ' a ' is the lattice parameter, u is the oxygen positional parameter, for ideal spinel ferrite $u = 3/8$ and the radius of oxygen ion, $R_o = 1.35$ Å. The hopping lengths in tetrahedral (L_A) and octahedral (L_B) sites have been calculated using the relation;

$$L_A = a(\sqrt{3}/4) \quad (3)$$

$$L_B = a(\sqrt{2}/4) \quad (4)$$

The calculated values of the various structural parameters are given in Table 1. The hopping lengths in the tetrahedral site (L_A) and in octahedral site (L_B) are the distance between the magnetic ions and were found to increase as the amount of zinc species increases resulting in magnetic dilution. Cobalt ferrite being an inverse spinel, the Fe^{3+} ions occupy both A and B sites, however, as more and more Zn^{2+} ions enter the A site, more Fe^{3+} ions occupy B sites which finally leads to magnetic isolation of the Fe^{3+} ions. It

Table 1 Lattice constant (a), ionic radii at tetrahedral site (r_A), ionic radii at octahedral site (r_B), tetrahedral bond length (A–O), octahedral bond length (B–O), Hopping lengths in tetrahedral (L_A) and octahedral

(L_B) of 'as prepared' and 'sintered' ferrite, $\text{Co}_{1-x}\text{Zn}_x\text{Fe}_2\text{O}_4$ ($x = 0.0-1.0$)

x	'As prepared'							'Sintered'						
	a (Å)	r_A (Å)	r_B (Å)	A–O (Å)	B–O (Å)	L_A (Å)	L_B (Å)	a (Å)	r_A (Å)	r_B (Å)	A–O (Å)	B–O (Å)	L_A (Å)	L_B (Å)
0.0	8.4867	0.4874	0.7717	1.926	2.072	3.675	3.004	8.4879	0.4877	0.7720	1.926	2.072	3.675	3.005
0.2	8.5129	0.4931	0.7782	1.932	2.078	3.686	3.014	8.5144	0.4934	0.7786	1.932	2.079	3.687	3.014
0.4	8.5272	0.4962	0.7818	1.935	2.082	3.692	3.019	8.5287	0.4965	0.7822	1.935	2.082	3.693	3.019
0.5	8.5363	0.4982	0.7841	1.937	2.084	3.696	3.022	8.5318	0.4972	0.7829	1.936	2.083	3.694	3.020
0.6	8.5378	0.4985	0.7844	1.938	2.085	3.697	3.023	8.5380	0.4985	0.7845	1.937	2.084	3.696	3.022
0.8	8.5537	0.5019	0.7884	1.941	2.088	3.704	3.028	8.5540	0.5020	0.7885	1.941	2.088	3.704	3.028
1.0	8.5628	0.5050	0.7919	1.945	2.093	3.711	3.033	8.5674	0.5049	0.7919	1.945	2.093	3.709	3.033

is also observed that the ionic radii (r_A , r_B) increase gradually with increase in the zinc content in the system, which in turn causes an increase in the lattice constant. The increase in r_A is due to the increasing amount of larger Zn^{2+} ions in the tetrahedral A site which consequently decreases the amount of Fe^{3+} ions in the A site. It can be concluded that the tetrahedral substitution plays dominant role in influencing the value of lattice constant. Similar findings on the nanocrystalline Co–Zn system have been reported by other investigators [13]. It can be understood that addition of Zn, i.e. tetrahedral substitution in the cobalt ferrite, induces structural changes without any crystal distortions as evident from the XRD powder patterns.

3.2 FTIR spectroscopy studies

The FTIR spectra of the ‘as prepared’ nanoferrite and the sintered ferrites are shown in Fig. 2a and b, respectively. Two main metal-oxygen bands are observed for all the studied spinel ferrite samples. The high frequency band in ferrites at 650 cm^{-1} (ν_1) is assigned to symmetrical vibrations of tetrahedral groups and the lower frequency band at $\sim 400\text{ cm}^{-1}$ (ν_2) is due to the vibrations of the octahedral M–O groups [25]. The difference in the band positions is due to the difference in the Fe^{3+} –O distances for octahedral and tetrahedral complexes. The ν_1 and ν_2 stretching vibration for the ‘as prepared’ oxide are observed between ~ 599 – 560 cm^{-1} and 420 – 399 cm^{-1} , respectively. Whereas for the sintered ferrites, the ν_1 and ν_2 vibrations are observed between 610 – 565 cm^{-1} and 435 – 410 cm^{-1} , respectively. As Co^{2+} gets replaced by Zn^{2+} , the ν_1 shifts to lower wavenumber as reported in the literature [25]. The gradual increase in broadening of the octahedral band for higher zinc concentration ($x > 0.5$) is related to the cation redistribution in the spinel structure. It is well known that zinc ions prefer to occupy tetrahedral sites, whereas, cobalt ions tend to prefer octahedral sites. The observed shift of the octahedral band with increasing zinc concentration indicates an increase in Fe^{3+} ions in the octahedral sites. This happens when the zinc ions enter tetrahedral A site and push the A site Fe^{3+} ions into the octahedral B site thereby replacing the cobalt ions at B sites. This process involving transfer of Fe^{3+} ions from A site to B site, decreases the wave number of the tetrahedral band [26]. Also, it is observed that the nanoferrites

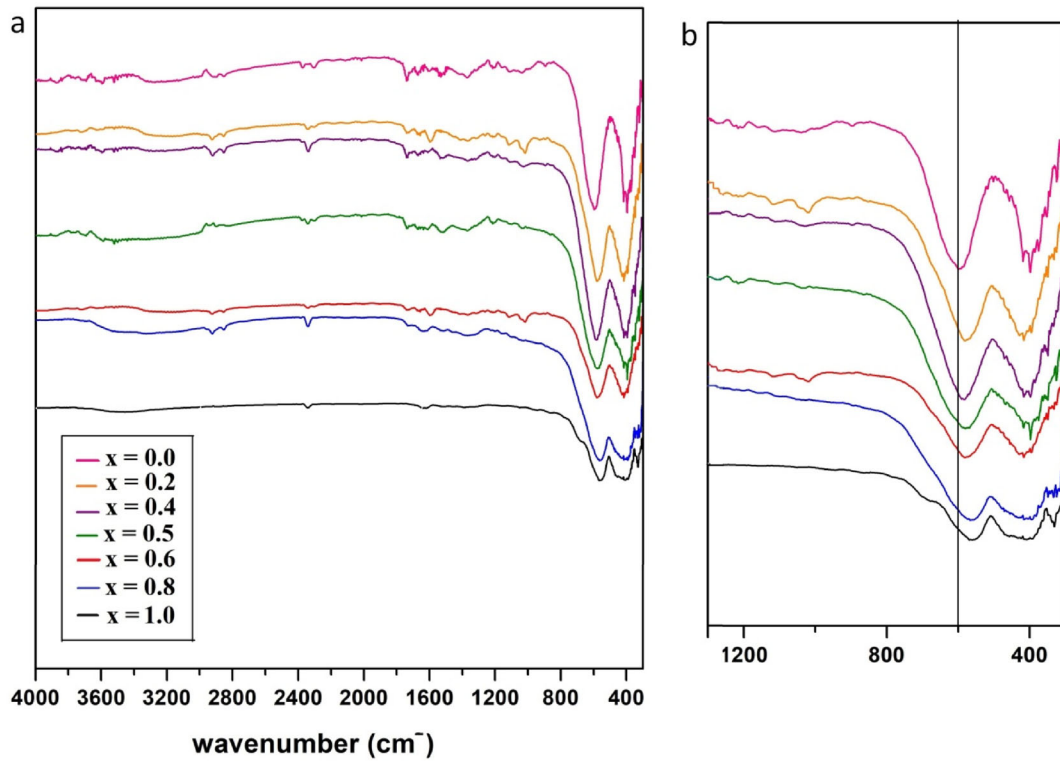
have slightly lower ν_1 and ν_2 values which shift to higher wavenumber upon increase in size. The weak bands at $\sim 3700\text{ cm}^{-1}$ and $\sim 1600\text{ cm}^{-1}$ in the sintered samples are attributed to O–H stretching vibration due to adsorbed water or moisture.

3.3 Surface area, particle size and morphology

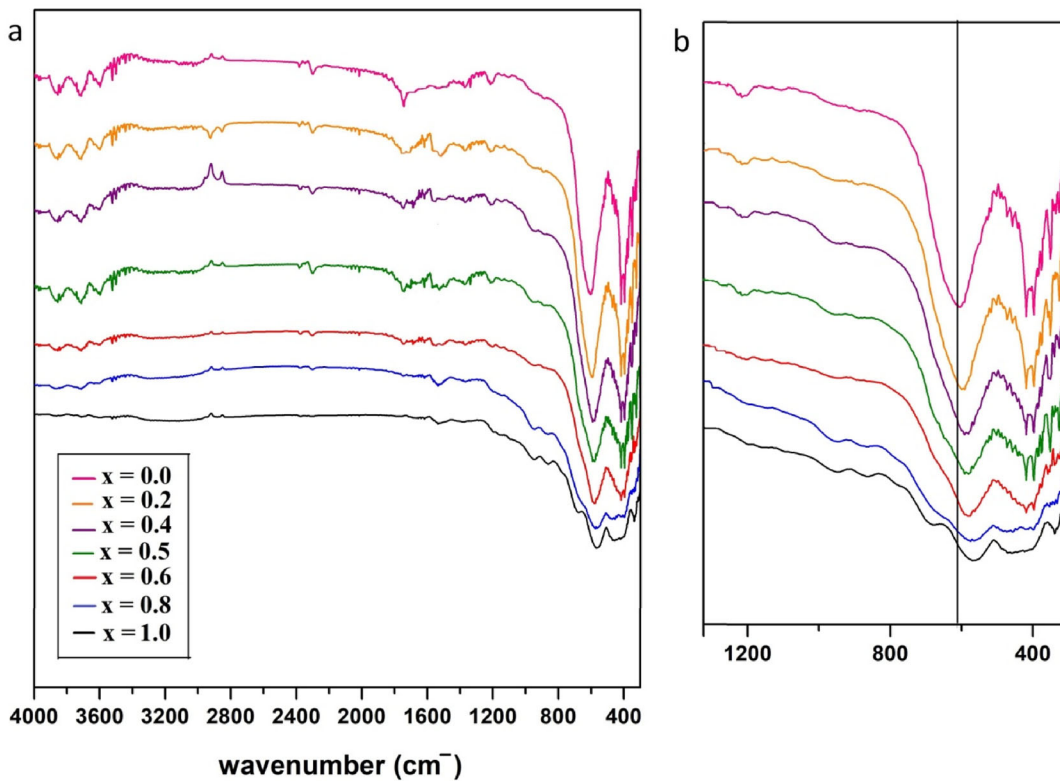
The morphology and the particle size of the ‘as prepared’ nanoferrites and bulk samples can be deduced from the TEM and SEM images, respectively. The TEM images, Fig. 3, of the ‘as prepared’ samples confirmed that the particles are nanosized in nature. Table 2 gives the particle size of the nanoferrites and sintered samples. The particle size for the ‘as prepared’ samples lies within 12–15 nm. It is also evident from the TEM images that the particles are agglomerated in appearance. Since the particles are magnetic in nature, a strong magnetic interaction is present which causes agglomeration. This was reflected in the BET surface area (Table 2). Sintering at $1000\text{ }^\circ\text{C}$ leads to coarsening of particles and an increase in grain size as seen in the SEM images (Fig. 4). The particle size for the sintered ferrites is in the range of 0.3 – $0.8\text{ }\mu\text{m}$. The specific BET surface area of the ‘as prepared’ nanoferrites is listed in Table 2 which is lower than expected due to the agglomeration of the particles as evident from the TEM images.

3.4 Magnetic studies

The AC magnetic susceptibility studies reveal the magnetic behavior of the material, i.e. ferrimagnetic to paramagnetic transition as well as the single domain to superparamagnetic transition. The domain structure and the Curie temperature were obtained by plotting normalized susceptibility against temperature. Figure 5 shows plots of thermal variation of normalized (χ_T/χ_{RT}) susceptibility for ‘as prepared’ and sintered samples which illustrate the above mentioned magnetic transition. The maximum in magnetization behavior just below the T_C in the presence of a small field is referred to as the Hopkinson effect [27–29] and has been observed for nanocrystalline single domain cobalt ferrite particles as well as nickel ferrite particles [30, 31]. In the case of cobalt ferrite and the mixed cobalt-zinc ferrite, there



a FTIR spectra of 'as prepared' $\text{Co}_{1-x}\text{Zn}_x\text{Fe}_2\text{O}_4$ ($x=0.0-1.0$).



b FTIR spectra of 'sintered' $\text{Co}_{1-x}\text{Zn}_x\text{Fe}_2\text{O}_4$ ($x=0.0-1.0$).

◀**Fig. 2 a** FTIR spectra of ‘as prepared’ $\text{Co}_{1-x}\text{Zn}_x\text{Fe}_2\text{O}_4$ ($x = 0.0\text{--}1.0$). **b** FTIR spectra of ‘sintered’ $\text{Co}_{1-x}\text{Zn}_x\text{Fe}_2\text{O}_4$ ($x = 0.0\text{--}1.0$)

is a slow increase in magnetization with temperature which reaches a maximum at temperature T_{max} , which is just below the Curie temperature. The maxima in the magnetization values (Hopkinson peak) and the corresponding temperature (T_{max}) are dependent on the applied field. The Hopkinson effect is observed in nanocrystalline single domain particles where the size of the particles is neither very small to be superparamagnetic nor very large to be multidomain in nature. The explanation for the Hopkinson effect in single domain cobalt ferrite nanoparticles is given by Ghajbhiye et al. [30]. In the present case, the Hopkinson peak is seen for the sintered samples where $x < 0.5$ and for some ‘as prepared’ samples indicating single domain nature of the particles. The susceptibility is inversely proportional to the coercive force. The existence of a coercive force indicates that the samples contain clusters of different sizes and each spin cluster is large when a high blocking temperature (T_{max}) is normally observed [32]. In this case, the T_{max} is quite large for samples with $x < 0.5$ indicating a higher coercive force. It is evident that as x increases the peak diminishes since the coercive force decreases. Addition of Zn into the cobalt ferrite reduces the coercive force and as a result, peak value decreases. If the temperature of a single domain particle is gradually increased at a constant magnetic field, it may so happen that the thermal energy may become comparable to the effective magnetic anisotropy when the magnetization direction spontaneously fluctuates between the easy axes of the grain. In such a state the particle will exhibit superparamagnetism. The temperature at which the single domain to superparamagnetic transition for a particle of volume V takes place is known as the blocking temperature (T_B) [32]. Superparamagnetic behavior is observed for samples with $x > 0.5$ whereas the samples having $x < 0.5$ are predominantly single domain in nature.

The Curie temperature, T_C is another vital parameter to study the size and interface effect on the ferrimagnetic phase transition and the magnetic phase stability of a material. The T_C of the ‘as prepared’ nanoferrite and the sintered ferrite values are listed in

Table 3. The observed decrease in T_C with small additions of zinc is due to the decreasing A–B superexchange interactions resulting from replacement of Fe^{3+} by Zn^{2+} at A sites [14]. Similar trend in behavior is reported by Gul et al. for Co–Zn ferrites of size 12.5–13 nm but the T_C values vary for certain compositions [8]. The reduction in T_C with increase in Zn content indicates a reduction in ferrimagnetic behavior. The Curie temperature values of the nano ‘as prepared’ ferrites are found to be lower than the sintered samples upto $x = 0.6$. A decrease in Curie temperature with particle size is reported for some cobalt zinc ferrite compositions by Veverka et al. [17]. It is incorrect to say that Curie temperature decreases with reduction in particle size since it may not be the case always. For single domain nanoparticles, the net alignment of atomic moments is dependent on the exchange interaction between the magnetic atoms of the particles. The strength of this interaction will determine the transition temperature. A stronger interaction means that more thermal energy will be needed to cause the moments to become disordered and the ferromagnetism to disappear, resulting in higher Curie temperature in nanoferrites [33]. Enhanced Curie temperature has also been reported for nanosized manganese ferrites [6]. Moreover, it is believed that the Curie temperature depends on the preparation conditions, measurement techniques and the applied field strength [13].

The effects of grain size reduction on the magnetic properties of ferrites were also investigated. In this respect, the measurements of coercive fields were particularly interesting. The coercivity of fine particles has a striking dependence on their size. As the particle size is reduced, it is typically found that the coercivity increases goes through a maximum and then tends towards zero. For a multidomain material, magnetization changes by domain wall motion. Below a critical diameter the particles become single domain and in this size range the coercivity reaches a maximum and changes their magnetization by spin rotation. As the particle size further decreases, the coercivity decreases and tends to zero because of thermal effects which are strong enough to spontaneously demagnetize a previously saturated assembly of particles. Such particles are called superparamagnetic [33]. The saturation magnetization (M_S), retentivity (M_R) and coercivity (H_C) values for ‘as prepared’ and sintered ferrites are listed in

Fig. 3 TEM images of ‘as prepared’ $\text{Co}_{1-x}\text{Zn}_x\text{Fe}_2\text{O}_4$ ($x = 0.2, 0.4, 0.5, 0.6, 0.8$) with SAED indexed pattern

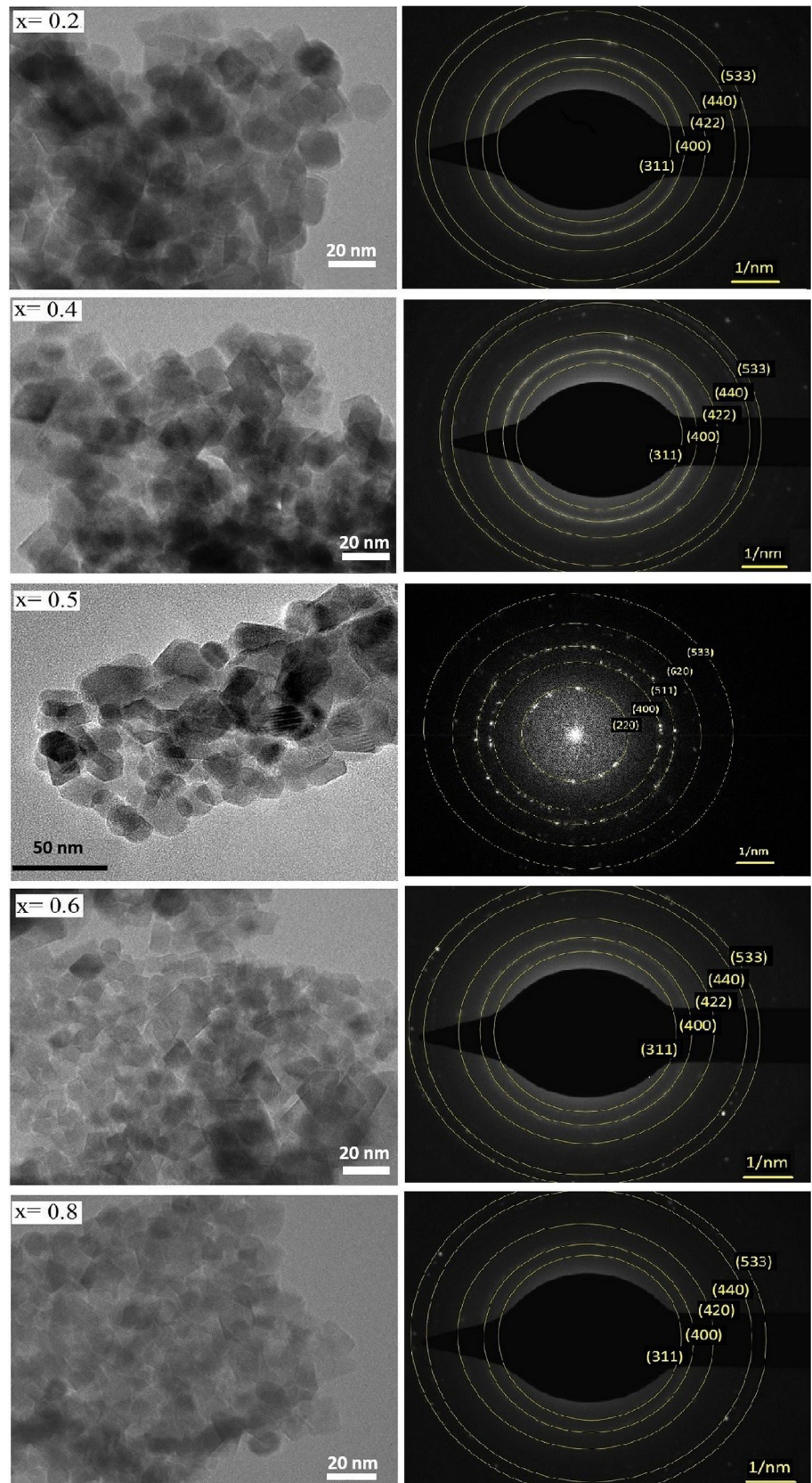


Table 2 Particle size (*t*) of ‘as prepared’ and ‘sintered’ ferrite, surface area (*SA*) of $\text{Co}_{1-x}\text{Zn}_x\text{Fe}_2\text{O}_4$ ($x = 0.0\text{--}1.0$)

<i>x</i>	‘As prepared’		‘Sintered’
	<i>t</i> (nm)	<i>SA</i> ($\text{m}^2 \text{g}^{-1}$)	<i>t</i> (μm)
0.0	–	32.7	0.5
0.2	14.7	23.2	0.3
0.4	14.4	23.6	0.4
0.5	12.9	42.4	0.4
0.6	13.3	36.6	0.8
0.8	12.5	32.3	0.2
1.0	–	19.8	0.3

Table 3. The ‘as prepared’ ferrites were found to have higher coercivity values than the sintered ferrites which reduce drastically with increasing Zn concentration. The coercivity is reported to decrease with decreasing concentration of cobalt as expected, due to higher magnetocrystalline anisotropy of Co^{2+} than Zn^{2+} ions. Considering all evidence, it appears that the nanoparticles are predominantly single domain in nature except for the samples with higher Zn concentration which show superparamagnetic effects. The domain nature of the ‘as prepared’ nanoferrites is confirmed by the temperature dependent magnetization studies.

The plots of Zero field-cooled (ZFC) and field-cooled (FC) magnetization as a function of temperature are shown in Fig. 6 for the ‘as prepared’ samples. The results are characteristic of magnetic nanoparticles with blocking temperature above room temperature. In a typical ZFC measurement, the nanoparticles were cooled from room temperature to 50 K without any external field and the magnetization was recorded during heating from 50 to 400 K under an applied field of 500 Oe. While in the FC measurement, the nanoparticles were cooled down to 50 K under the applied field of 500 Oe and the magnetization was recorded during heating till 400 K under an applied field of 500 Oe. The ZFC magnetization (M_{ZFC}) increased as the temperature increased from 50 K and reached a maximum corresponding to the blocking temperature (T_{B}) and then decreased, whereas the FC magnetization (M_{FC}) steadily decreased as the temperature increased from 50 K. Above T_{B} , the so called unblocked region, the M_{ZFC} decreased gradually with increasing temperature

wherein the spins become disordered and achieve superparamagnetism. However, a continuous decrease in M_{FC} was observed with increasing temperature indicating thermal vibration leading to randomization of nanoparticles in FC measurement. As can be seen from Fig. 6, only the nanoparticles with Zn concentration $x > 0.5$, exhibits superparamagnetism at room temperature. The blocking temperature shifts towards higher temperature for $x \leq 0.5$, where the superparamagnetic behavior is seen above room temperature. The difference between M_{ZFC} and M_{FC} curves below T_{B} mainly results from the existence of energy barriers of magnetic anisotropy [34, 35]. Although the ‘as prepared’ ferrite have a particle size between 12 and 15 nm and are predominantly single domain in nature, apparently, it has not lost the magnetic ordering to exhibit room temperature superparamagnetism, especially the compositions with $x \leq 0.5$.

Figures 7 and 8 show the room temperature hysteresis of the ‘as prepared’ and sintered $\text{Co}_{1-x}\text{Zn}_x\text{Fe}_2\text{O}_4$ ($x = 0.0\text{--}1.0$). The lower values of saturation magnetization in nanoparticles of the ‘as prepared’ ferrite as compared to the submicron particles of the sintered samples is attributed to the surface effects which lead to the noncollinearity of the magnetic moments on their surface and can be explained in terms of core shell model of the nanoparticles in which the core contains ferrimagnetically aligned spins on the surface or interface with a certain degree of spin canting [36]. It is seen that the M_{S} values initially increase upto $x = 0.4$ and then decrease with increasing Zn concentration (Table 3). The $\text{Co}_{1-x}\text{Zn}_x\text{Fe}_2\text{O}_4$ are largely inverse spinel for $x = 0$ which can be represented as $[\text{Fe}^{3+}]^{\text{tet}}[\text{Co}^{2+} \text{Fe}^{3+}]^{\text{oct}}\text{O}_4$, while the zinc ferrite ($x = 1.0$) is a normal spinel at room temperature, $[\text{Zn}^{2+}]^{\text{tet}}[\text{Fe}_2^{3+}]^{\text{oct}}\text{O}_4$. The spins of the Fe^{3+} ions on the octahedral sites of ZnFe_2O_4 are not aligned but are random. Therefore, ZnFe_2O_4 is paramagnetic and shows no saturation magnetization. On formation of the mixed cobalt zinc ferrite by partial replacement of Co^{2+} by Zn^{2+} , a gradual change from inverse to normal behavior is found to occur. Introduction of Zn^{2+} into the tetrahedral sites causes Fe^{3+} ions to be displaced on the octahedral sites, i.e. $[\text{Fe}_{1-x}^{3+} \text{Zn}_x^{2+}]^{\text{tet}}[\text{Co}_{1-x}^{2+} \text{Fe}_{1+x}^{3+}]^{\text{oct}}\text{O}_4$. If the mixed cobalt zinc ferrite retained the antiferromagnetic character of the $\text{Co}_{1-x}\text{Zn}_x\text{Fe}_2\text{O}_4$ ($x = 0$), a linear increase in M_{S} should occur and attain a maximum

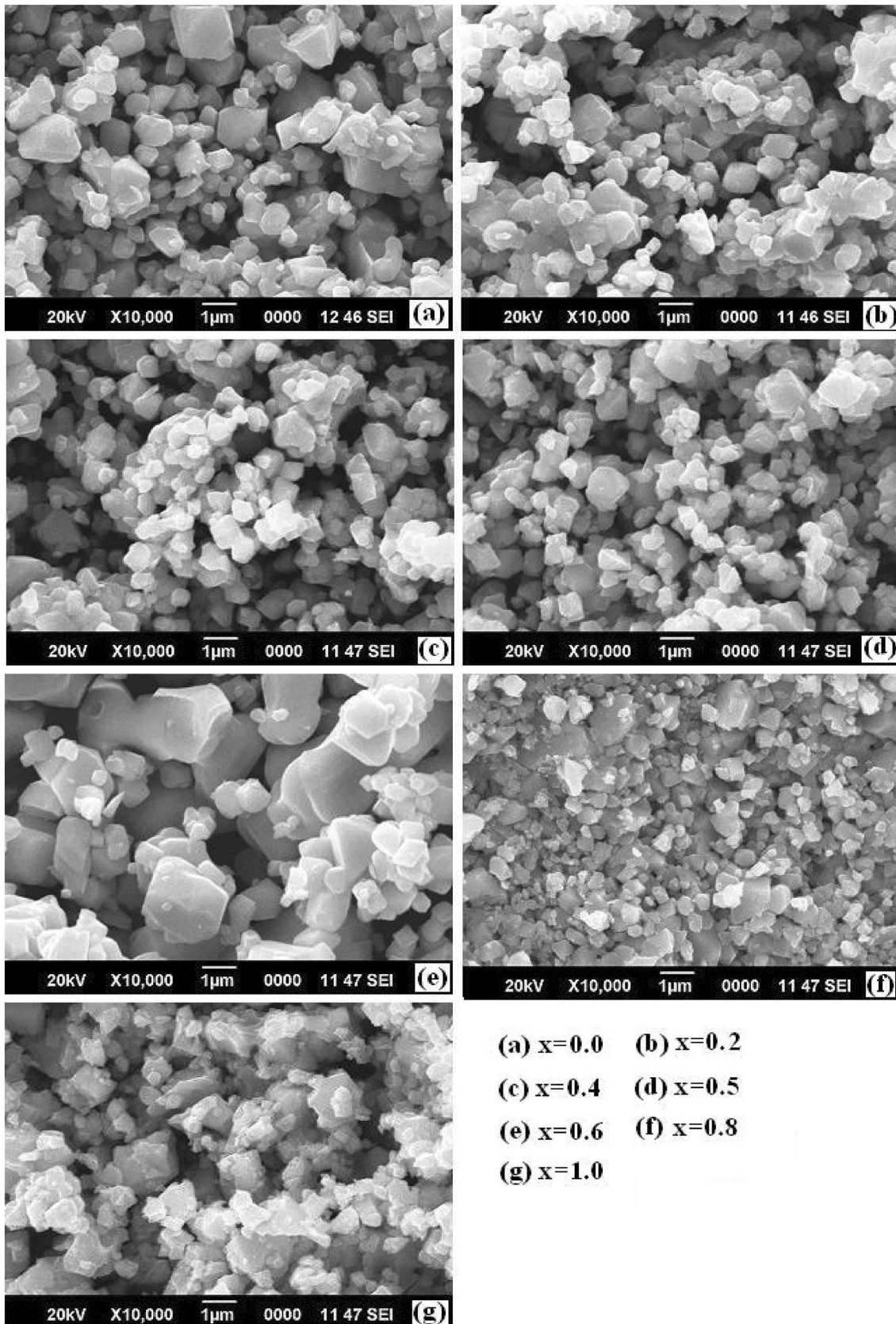


Fig. 4 SEM images of 'sintered' $\text{Co}_{1-x}\text{Zn}_x\text{Fe}_2\text{O}_4$ ($x = 0.0\text{--}1.0$)

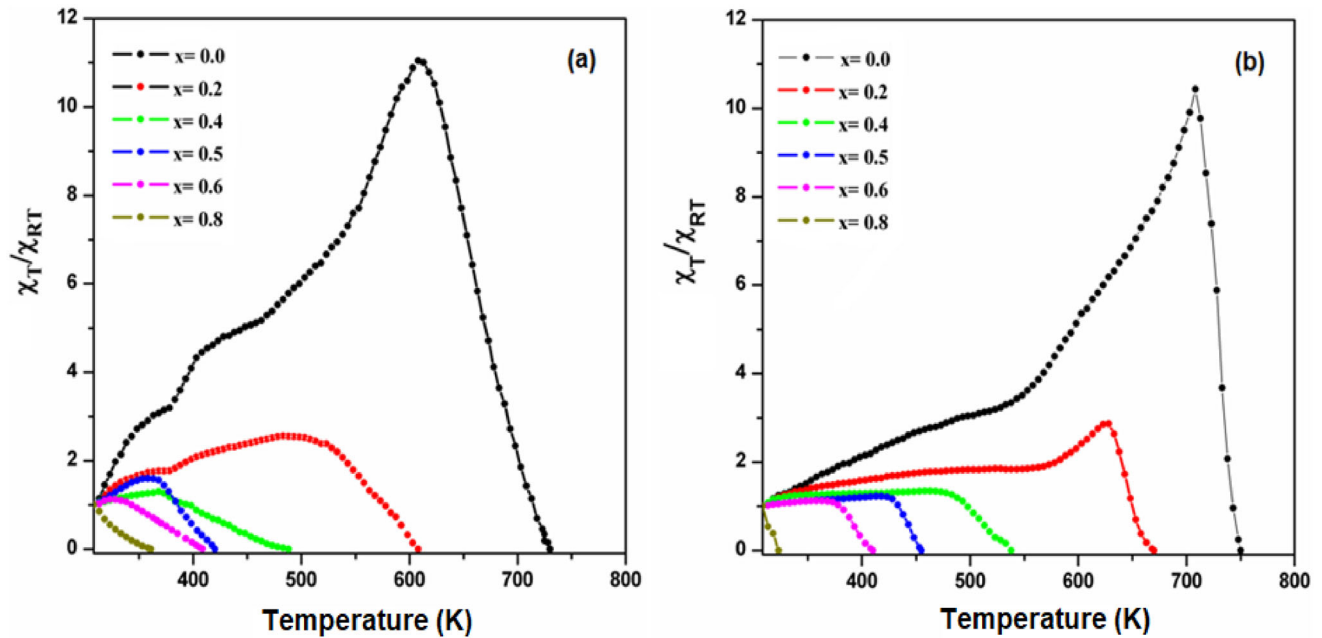


Fig. 5 Effect of Zn substitution on the temperature dependent susceptibility of **a** ‘as prepared’ and **b** ‘sintered’ $\text{Co}_{1-x}\text{Zn}_x\text{Fe}_2\text{O}_4$ ($x = 0.0\text{--}0.8$)

Table 3 Saturation magnetization, M_S (emu/g); Retentivity, M_R (emu/g); Coercivity, H_C (emu/g); Curie temperature, T_C (°K) of ‘as prepared’ and ‘sintered’ ferrite, $\text{Co}_{1-x}\text{Zn}_x\text{Fe}_2\text{O}_4$ ($x = 0.0\text{--}1.0$)

x	‘As prepared’				‘Sintered’			
	M_S (emu/g)	M_R (emu/g)	H_C (emu/g)	T_C (°K)	M_S (emu/g)	M_R (emu/g)	H_C (emu/g)	T_C (°K)
0.0	52.28	23.24	1249.6	730	81.97	23.36	496.98	750
0.2	65.97	17.09	316.6	608	88.73	13.13	255.42	670
0.4	79.59	9.40	133.02	488	90.85	6.36	168.27	538
0.5	59.90	6.33	63.60	420	70.20	3.18	33.74	455
0.6	47.70	2.34	27.00	409	67.72	1.55	25.96	410
0.8	9.80	0.58	10.60	361	5.91	0.11	10.14	323
1.0	3.50	0.27	67.00	–	7.18	1.80	96.45	–

for $x = 1.0$. However, long before $x = 1.0$ is reached, the antiferromagnetic coupling is destroyed and the M_S values drop [37]. As observed from the magnetization studies, M_S increases for small values of x , but pass through a maximum for $x = 0.4$ and then decreases. According to Neel’s collinear two sub lattice model [38], the saturation magnetization moment of spinel ferrite can be expressed as $M_S = M_B - M_A$ where M_A and M_B are net magnetic moment of tetrahedral (A) and octahedral (B) sublattice, respectively. Zn^{2+} ions with zero magnetic moment replace ions on the tetrahedral A sites, causing the decrease of magnetic moment in this sub lattice M_A resulting in the increase of the total magnetic moment, M . Due to the replacement of Fe^{3+} at the tetrahedral sites and

the prominent inter-sublattice A–B superexchange interaction, the net magnetic moment per formula unit is increased, hence M_S increases. The Neel’s collinear two sub lattice model gives an account for the initial increase but is unable to explain the subsequent decrease. However, the decrease can be explained in terms of a uniform Yafet–Kittel triangular type magnetic ordering of spins on the B sub lattice [39]. But for a mixed system like Co–Zn ferrite, it is quite possible that the canting is not uniform but instead is locally dependent upon the statistical distribution of non-magnetic neighboring ions. Therefore, the decrease in magnetization of these compositions after $x = 0.4$ is attributed to the canting of the magnetic moments. A maximum M_S value of

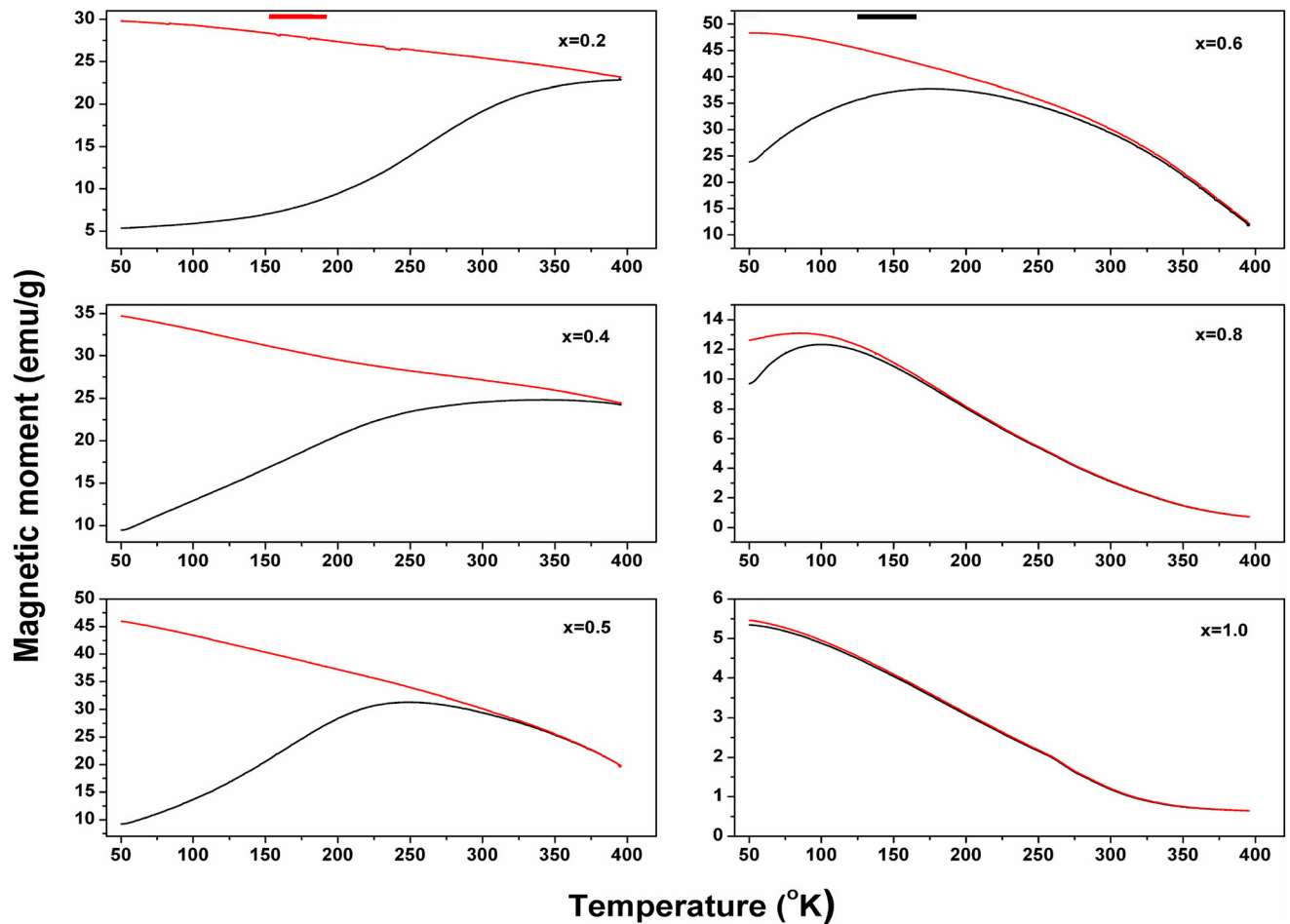


Fig. 6 Field cooled (FC) and Zero field cooled (ZFC) magnetisations as a function of temperature for $\text{Co}_{1-x}\text{Zn}_x\text{Fe}_2\text{O}_4$ ($x = 0.0$ – 1.0) nanoparticles under an applied field of 500 Oe

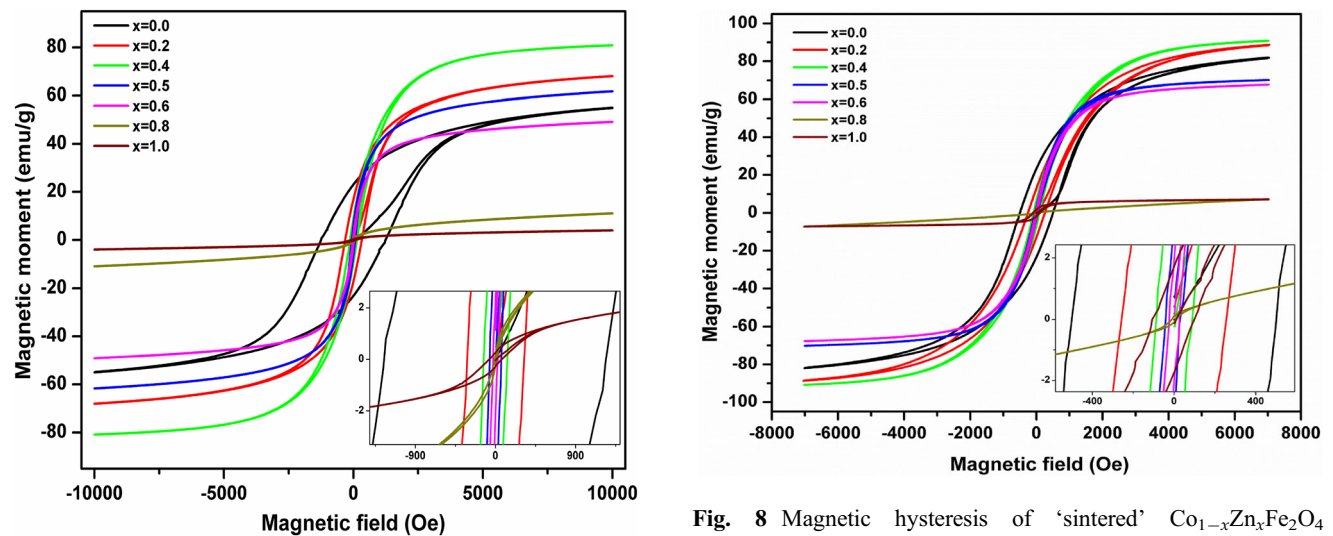


Fig. 7 Magnetic hysteresis of ‘as prepared’ $\text{Co}_{1-x}\text{Zn}_x\text{Fe}_2\text{O}_4$ ($x = 0.0$ – 1.0)

Fig. 8 Magnetic hysteresis of ‘sintered’ $\text{Co}_{1-x}\text{Zn}_x\text{Fe}_2\text{O}_4$ ($x = 0.0$ – 1.0)

90.85 emu/g and 79.59 emu/g for $x = 0.4$ was obtained for the sintered and ‘as prepared’ sample, respectively.

3.5 Mössbauer spectroscopy

The Mössbauer spectroscopy is a useful technique to study the magnetic nature of the ferrites and to get a closer view of the superparamagnetic behavior of the nanocrystals. It also gives a fair idea about the cation distribution as well as the oxidation state of the Fe ion. The experimental observations obtained from the magnetic measurements of ‘as prepared’ and sintered Co–Zn ferrite are in agreement with the Mössbauer data. Figures 9 and 10 compares the room

temperature Mössbauer spectra of the ‘as prepared’ and sintered $\text{Co}_{1-x}\text{Zn}_x\text{Fe}_2\text{O}_4$ respectively, with x varying from 0 to 1. The spectral parameters of the sintered and ‘as prepared’ nanoferrite {isomer shift (δ), quadrupole splitting (Δ), line width (Γ), hyperfine magnetic field (H_{hf}) and relative area (R_A) in percentage in tetrahedral and octahedral sites of Fe^{3+} ions} are summarized in Table 4. There are superposition of two sextets and a doublet pattern for ‘as prepared’ ($x = 0.6$) and sintered ferrite ($x = 0.5$ and 0.6). Doublet pattern arises from the presence of superparamagnetic fraction whereas the sextet or Zeeman splitting pattern is due to the presence of ferrimagnetic fraction. Outer (higher hyperfine field) and inner (lower hyperfine field) sextets correspond

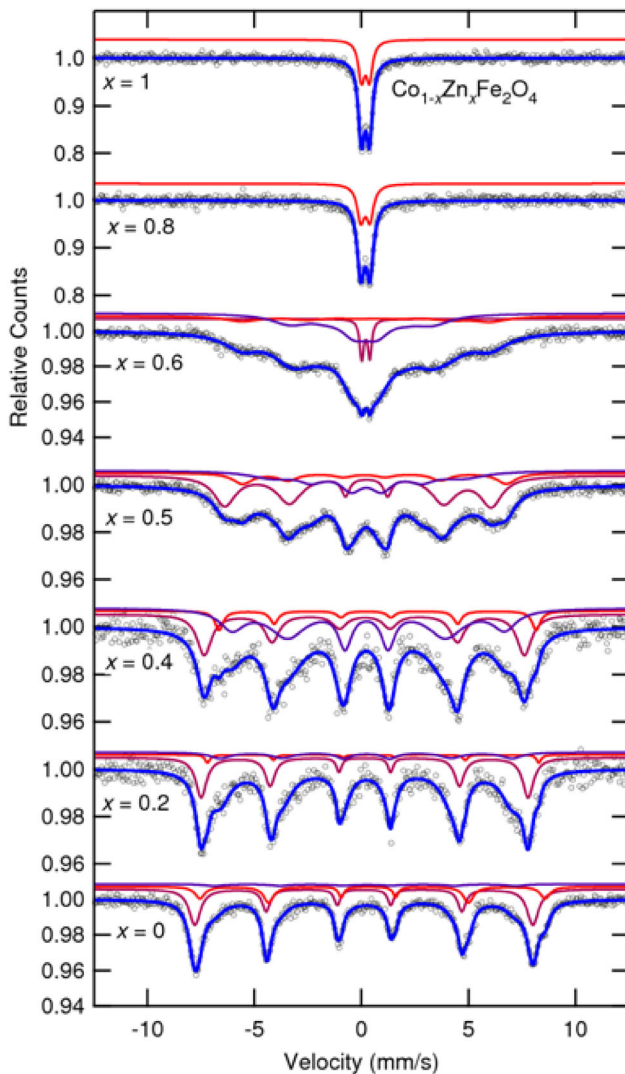


Fig. 9 Mössbauer spectra of ‘as prepared’ $\text{Co}_{1-x}\text{Zn}_x\text{Fe}_2\text{O}_4$ ($x = 0.0$ – 1.0)

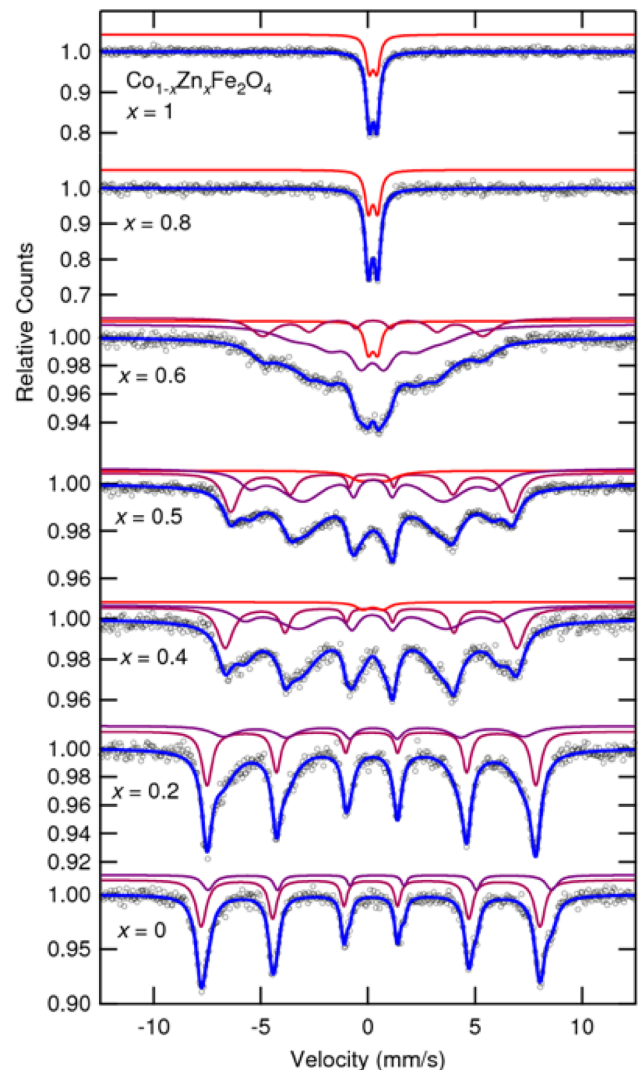


Fig. 10 Mössbauer spectra of ‘sintered’ $\text{Co}_{1-x}\text{Zn}_x\text{Fe}_2\text{O}_4$ ($x = 0.0$ – 1.0)

Table 4 Isomer shift (IS), quadruple splitting (QS), hyperfine field (H_{hf}), inner line width (Γ), relative Area (R_A) of ‘as prepared’ and ‘sintered’ ferrite, $\text{Co}_{1-x}\text{Zn}_x\text{Fe}_2\text{O}_4$

Zn	‘As prepared’						‘Sintered’					
	Fe sites	IS(δ) (mm/s)	QS(Δ) (mm/s)	H_{hf} (KG)	Γ (mm/s)	R_A (%)	IS(δ) (mm/s)	QS(Δ) (mm/s)	H_{hf} (KG)	Γ (mm/s)	R_A (%)	
0.0	Sextet A	0.119	− 0.009	489.8	0.343	51.7	0.13	− 0.011	490.3	0.341	77	
	Sextet B	0.425	0.190	500.3	0.298	22.1	0.492	0.133	497.4	0.29	23	
	Sextet B1	0.212	− 0.091	436.4	0.538	26.1	–	–	–	–	–	
0.2	Sextet A	0.155	− 0.006	473.8	0.279	41.0	0.266	0.018	435.6	0.612	50.7	
	Sextet B	0.461	− 0.174	480.0	0.263	3.7	0.172	− 0.009	476	0.359	49.3	
	Sextet B1	0.227	− 0.034	422.8	0.838	55.3	–	–	–	–	–	
0.4	Sextet A	0.147	− 0.018	464.0	0.828	37.3	0.193	− 0.021	368.8	0.744	76.2	
	Sextet B	0.485	0.547	459.5	0.453	5.3	0.113	0.07	422.1	0.322	21.2	
	Sextet B1	0.282	0.084	0.395	0.765	57.4	0.23	0.941	–	0.78	2.6	
0.5	Sextet A	0.041	− 0.400	386.1	0.452	29.9	0.202	–	351.7	0.542	72.8	
	Sextet B	0.369	0.483	382.4	1.064	19.5	0.171	− 0.002	407.4	0.292	18.6	
	Sextet B1/Doublet	0.252	0.030	276.9	1.250	50.6	0.258	1.19	–	1.27	8.6	
0.6	Sextet A	0.085	− 0.210	205.2	1.592	67.9	0.136	− 0.152	214.9	1.09	81.2	
	Sextet B	0.516	− 0.600	360.0	1,979	31.3	0.238	− 0.019	318.8	0.521	16.4	
	Doublet	0.205	0.374	–	0.219	0.8	0.237	0.432	–	0.453	2.4	
0.8	Doublet	0.185	0.427	–	0.405	100	0.235	0.421	–	0.371	100	
1.0	Doublet	0.189	0.372	–	0.345	100	0.24	0.346	–	0.352	100	

Sextet A: Tetrahedral, Sextet B: Octahedral

to Fe^{3+} ions in octahedral and tetrahedral sites, respectively in the $\text{Co}_{1-x}\text{Zn}_x\text{Fe}_2\text{O}_4$ ferrite [40–42]. With addition of Zn, there is a reduction in H_{hf} as compared to CoFe_2O_4 . It is evident that, with the increasing zinc concentration, there is a transition from magnetically ordered ferrimagnetic state (characterized by a sextet) to a paramagnetic state (characterized by a doublet). This behavior is expected when diamagnetic Zn^{2+} ions substitute the magnetic Co^{2+} ions [43]. The Mössbauer spectra agrees with the magnetization data, as x increases, coercivity decreases which is also found to be high for ‘as prepared’ cobalt ferrite as compared to the sintered ones. The Mössbauer spectra of the nanoferrites (Fig. 9) are marked by the presence of three magnetically split sextets for $x = 0, 0.2, 0.4$, and 0.5 . Sextet A (with lower δ value) belongs to tetrahedral site whereas sextet B (with higher δ value) and B1 belong to octahedral site [44–46]. The relative area of the central paramagnetic doublet increases whereas the relative area of magnetic sextets decreases with increase in the zinc content. The area of the doublet increases drastically beyond $x > 0.6$. Only a single doublet is present for composition $x = 0.8$ and 1.0 for both nanosize and

sintered samples as shown in Figs. 9 and 10. The Mössbauer spectra of the sintered (Fig. 10) ferrites exhibit two normal Zeeman-split sextets for $x = 0.0$ – 0.2 , one due to Fe^{3+} ions at the tetrahedral (A) sites and the other due to the Fe^{3+} ions at the octahedral (B) sites. The spectrum obtained for the composition with $x = 0.4, 0.5$ and 0.6 shows broad sextet features of relaxation effect, and a central paramagnetic doublet resulting from superparamagnetic Fe^{3+} species [46–50]. The samples with $x \geq 0.8$ exhibit paramagnetic spectra with only a central doublet. Like in the nanosize samples, the relative intensity of the central doublet was also found to increase with the concentration of Zn^{2+} in the sintered samples. The central doublet can be attributed to the magnetically isolated Fe^{3+} ions which do not participate in the long-range magnetic ordering due to a large number of nonmagnetic nearest neighbors. It can be observed that, for ‘as prepared’ and sintered ferrites, the magnitude of magnetic hyperfine fields of A site (H_A) and B site (H_B) decrease as the Zn content increases (Fig. 11). Also, the hyperfine field of A site (H_A) decreases more rapidly than that of B site. The rapid decrease of the magnetic hyper-fine field of

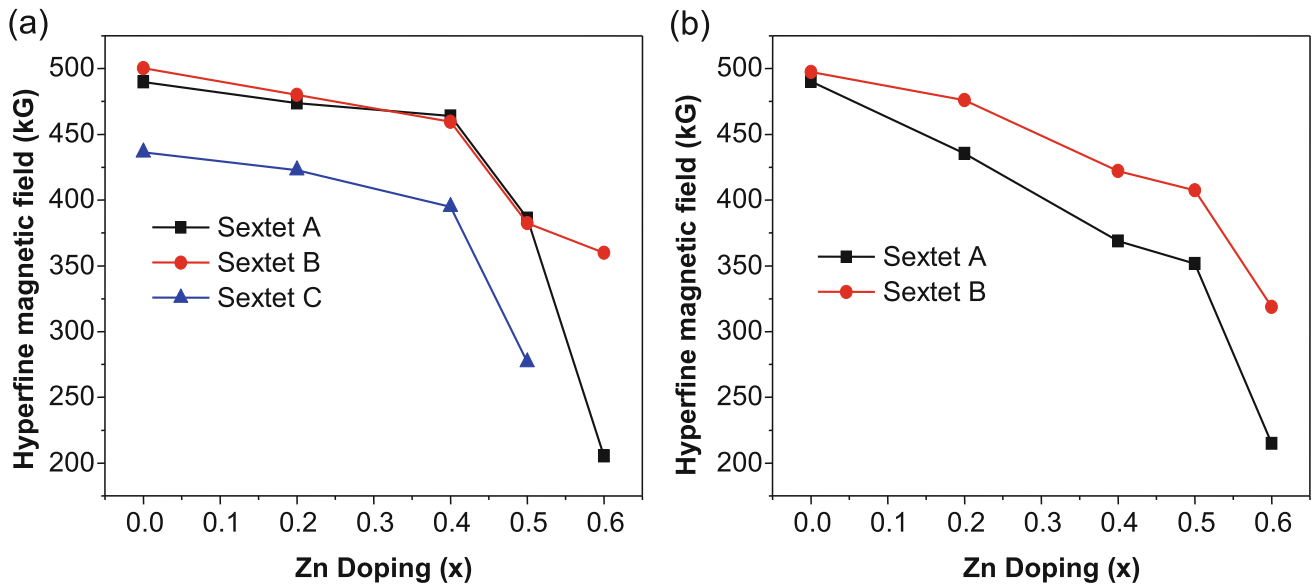


Fig. 11 Variation in hyperfine magnetic field of **a** 'as prepared' and **b** 'sintered' Co_{1-x}Zn_xFe₂O₄ ($x = 0.0-1.0$) with Zn doping

A site with increasing Zn content is attributed to the dilution of the field component from Fe³⁺ ions in the A site [12]. These experimental observations support the theoretical calculations carried out to determine the distance between the magnetic ions (L_A and L_B) based on the lattice parameters. Thus, the nanosize ferrites acquire a doublet character indicative of a superparamagnetic state in the dominant part of the particles as compared to the sintered ferrites, wherein the sextet is retained although the respective hyperfine fields are largely reduced and broadly distributed for the A and B sites [17]. Isomer shift (δ) values for all compositions of x of 'as prepared' and sintered samples (δ value between 0.041–0.492 mm/s) indicate that Fe is in Fe³⁺ ionic state [46, 51–53]. This ranges of δ also supports the absence of Fe²⁺ ion in these samples because the Fe²⁺ ions show much higher value of δ ($\delta \geq 0.8$ mm/s). The change in δ values of nanoferrites relative to the sintered samples is attributed to the change in the Fe³⁺–O²⁻ distance at the A and B sites due to crystal distortion. When the distance of the ligand oxygen to iron is shorter in the oxygen polyhedra, greater is the s-electron density at the Fe-nucleus, which results in lowering of isomer shift and vice versa [44, 54]. However, the mid-compositions of nanoferrites particularly $x = 0.5$ and $x = 0.6$ show a slight anomaly, their δ values being higher than the bulk. This anomaly is attributed to the preparation condition and subsequent heat treatment. Quadrupole splitting (Δ) values for all x values of doublet for 'as prepared' and sintered

ferrite with respect to α -Fe suggest that Fe³⁺ ions show asymmetry of polyhedron. Δ values for tetrahedral and octahedral sites, for the 'as prepared' and sintered samples are nearly 0.00 mm/s suggesting that Fe³⁺ ions show cubic symmetry of polyhedron.

4 Conclusions

The precursor combustion method offers a convenient route for preparing magnetic nanoparticles of cobalt zinc ferrite with tuneable properties. We have demonstrated that the magnetic properties of cobalt ferrite can be suitably controlled by substituting Co²⁺ with the non-magnetic Zn²⁺ ion even at the nanoscale. The addition of non-magnetic Zn²⁺ ions leads to magnetic dilution at the lattice sites thus affecting the magnetic properties considerably. From the study of 'as prepared' (nano) and sintered (bulk) ferrites the behavior of the material with respect to the particle size is well understood. The particle size invariably influences the structure, cation distribution, domain nature and the magnetic ordering present in the ferrite samples. Superparamagnetic features were noticeable only in some of the 'as prepared' samples since the nanoferrites have not yet reached the critical size to exhibit superparamagnetism. The critical dimensions required for the nanoparticles to lose the magnetic ordering and manifest superparamagnetism needs further investigation.

Author contributions

All authors contributed to the study conception and design. Material preparation, data collection and analysis were performed by LRG and VMSV. SGG and SSM carried out VSM magnetic measurements and Mossbauer studies, respectively. The first draft of the manuscript was written by LRG and all authors commented on previous versions of the manuscript. All authors read and approved the final manuscript.

Funding

The authors declare that no funds, Grants, or other support received during preparation of this manuscript.

Data availability

The data sets generated during and/or analyzed during the current study are available from the corresponding author on reasonable request.

Declarations

Conflict of interest On behalf of all authors, the corresponding author states that there is no conflict of interest.

Ethical approval The authors declare that the ethical standards are maintained while writing this manuscript.

References

- P.A. Rao, K.S. Rao, T.R.K. Pydi Raju, G. Kapusetti, M. Choppadandi, M.C. Varma, K.H. Rao, J. Alloy Compd. **794**, 60 (2019)
- T. Tatarchuk, A. Shyichuk, Z. Sojka, J. Gryboś, M. Naushad, V. Kotsyubynsky, M. Kowalska, S. Kwiatkowska-Marks, N. Danyliuk, J. Mol. Liq. **328**, 115375 (2021)
- N.K. Yetim, E.H. Ozkan, J. Mater. Sci.: Mater. Electron. **32**, 24766 (2021)
- E.A. Schultz-Sikma, H.M. Joshi, Q. Ma, K.W. MacRenaris, A.L. Eckermann, V.P. Dravid, T.J. Meade, Chem. Mater. **23**, 2657 (2011)
- D. Makovec, A. Kosak, A. Znidarsic, M. Drogenik, J. Magn. Magn. Mater. **289**, 32 (2005)
- Z.X. Tang, C.M. Sorensen, K.J. Klabunde, G.C. Hadjipanyis, Phys. Rev. Lett. **67**, 3602 (1991)
- R.H. Kodama, A.E. Berkowitz, E.J. McNiff, S. Goner, Phys. Rev. Lett. **77**, 394 (1996)
- I.H. Gul, A.Z. Abbasi, F. Amin, M. Anis-ur-Reehman, A. Maqsood, J. Magn. Magn. Mater. **311**, 494 (2007)
- M. Sedlacik, V. Pavlinek, P. Peer, P. Filip, Dalton Trans. **43**, 6919 (2014)
- A.J. Rondinone, A.C.S. Samia, Z. John Zhang, Appl. Phys. Lett. **76**, 3624 (2000)
- N. Bao, L. Shen, Y.A. Wang, J. Ma, D. Mazumdar, A. Gupta, J. Am. Chem. Soc. **131**, 12900 (2009)
- W. Bayoumi, J. Mater. Sci. **42**, 8254 (2007)
- N.M. Deraz, A. Alarifi, J. Anal. Appl. Pyrol. **94**, 41 (2012)
- S.S. Jadhav, S.E. Shirsath, S.M. Patange, K.M. Jadhav, J. Appl. Phys. **108**, 093920 (2010)
- V.G. Patil, S.E. Shirsath, S.D. More, S.J. Shukla, K.M. Jadhav, J. Alloy Compd. **488**, 199 (2009)
- B. Vishwanathan, V.R.K. Murthy, *Ferrite Materials, Science and Technology* (Narosa Publishing House, New-Delhi, 1990)
- M. Veverka, Z. Jirak, O. Kaman, K. Knizek, M. Marysko, E. Pollert, K. Zaveta, A. Lancok, M. Dlouha, S. Vratislav, Nanotechnology **22**, 345701 (2011)
- M. George, S.S. Nair, K.A. Malini, P.A. Joy, M.R. Anantharaman, J. Phys. D: Appl. Phys. **40**, 1593 (2007)
- C. Rath, S. Anand, R.P. Das, K.K. Sahu, S.D. Kulkarni, S.K. Date, N.C. Mishra, J. Appl. Phys. **91**, 2211 (2002)
- R.B. Kamble, V. Varade, K.P. Ramesh, V. Prasad, AIP Adv. **5**, 017119 (2015)
- Q. Li, C.W. Kartikowati, S. Horie, T. Ogi, T. Iwaki, K. Okuyama, Sci. Rep. **7**, 9894 (2017)
- L.R. Gonsalves, S.C. Mojumdar, V.M.S. Verenkar, J. Therm. Anal. Calorim. **100**, 789 (2010)
- F.J. Owens, C.P. Poole Jr., *The Physics and Chemistry of Nano solids* (Wiley, New Jersey, 2008)
- M. Veverka, P. Veverka, Z. Jirak, O. Kaman, K. Knizek, M. Marysko, E. Pollert, K. Zaveta, J. Magn. Magn. Mater. **322**, 2386 (2010)
- R.D. Waldron, Phys. Rev. **99**, 1727 (1955)
- V. Mameli, A. Musinu, A. Ardu, G. Ennas, D. Peddis, D. Niznansky, C. Sangregorio, C. Innocenti Nguyen, T.K. Thanh, C. Cannas, Nanoscale **19**, 10124 (2016)
- O. Popov, P. Rachev, M. Mikhov, F. Calderon, J.L. Sanchez, F. Leccabue, J. Magn. Magn. Mater. **99**, 119 (1991)
- E.C. Stoner, E.P. Wohlfarth, Phil. Trans. R. Soc. A **240**, 599 (1948)
- H. Pfeiffer, W. Schuppel, J. Magn. Magn. Mater. **130**, 92 (1994)

30. N.S. Gajbhiye, S. Prasad, G. Balaji, IEEE Trans. Magn. **35**, 2155 (1999)
31. S. Prasad, N.S. Gajbhiye, J. Alloy Compd. **265**, 87 (1998)
32. C.P. Bean, J. Appl. Phys. **26**, 1381 (1955)
33. B.D. Cullity, C.D. Graham, *Introduction to Magnetic Materials* (Wiley-IEEE Press, New Jersey, 2008)
34. T. Hyeon, Y. Chung, J. Park, S.S. Lee, Y. Kim, B.H. Park, J. Phys. Chem. B **106**, 6831 (2002)
35. S.G. Gawas, S.S. Meena, P. Bhatt, V.M.S. Verenkar, Mater. Chem. Front. **2**, 300 (2018)
36. A. Ghasemi, V. Sepelak, S.E. Shirsath, X. Liu, A. Morisako, J. Appl. Phys. **109**, 07A512 (2011)
37. A.R. West, *Solid State Chemistry and Its Applications* (Wiley, India, 2003)
38. L. Neel, C. R. Acad. Sci. Paris **230**, 375 (1950)
39. Y. Yafet, C. Kittel, Phys. Rev. **87**, 290 (1952)
40. G.A. Petitt, D.W. Forester, Phys. Rev. B **4**, 3912 (1971)
41. R. Shukla, R.S. Ningthoujam, S.S. Umare, S.J. Sharma, S. Kurian, R.K. Vatsa, A.K. Tyagi, N.S. Gajbhiye, Hyperfine Interact. **184**, 217 (2008)
42. H.H. Joshi, P.B. Pandya, R.G. Kulkarni, Solid State Comm. **86**, 807 (1993)
43. S.K. Kulshreshtha, J. Mater. Sci. Lett. **5**, 638 (1986)
44. S.S. Shinde, S.S. Meena, S.M. Yusuf, K.Y. Rajpure, J. Phys. Chem. C **115**, 3731 (2011)
45. S.R. Naik, A.V. Salker, S.M. Yusuf, S.S. Meena, J. Alloy Compd. **566**, 54 (2013)
46. K. Vasundhara, S.N. Achary, S.K. Deshpande, P.D. Babu, S.S. Meena, A.K. Tyagi, J. Appl. Phys. **113**, 194101 (2013)
47. A. Mitra, J. Mohapatra, S.S. Meena, C.V. Tomy, M. Aslam, J. Phys. Chem. **118**, 19356 (2014)
48. R. Ghosh, L. Pradhan, Y.P. Devi, S.S. Meena, R. Tewari, A. Kumar, S. Sharma, N.S. Gajbhiye, R.K. Vatsa, B.N. Pandey, R.S. Ningthoujam, J. Mater. Chem. **21**, 13388 (2011)
49. S.M. Patange, S.S. Desai, S.S. Meena, S.M. Yusuf, S.E. Shirsath, RSC Adv. **5**, 91482 (2015)
50. U.B. Gawas, V.M.S. Verenkar, S.R. Barman, S.S. Meena, P. Bhatt, J. Alloy Compd. **555**, 225 (2013)
51. K. Sharma, S.S. Meena, S. Saxena, S.M. Yusuf, A. Srinivasan, G.P. Kothiyal, Mater. Chem. Phys. **133**, 144 (2012)
52. K. Sharma, S. Singh, C.L. Prajapat, S. Bhattacharya, M.R. Jagannath, S.M. Singh, G.P. Yusuf, Kothiyal, J. Magn. Magn. Mater. **321**, 3821 (2009)
53. K. Sharma, A. Dixit, S. Singh, S. Jagannath, C.L. Bhattacharya, P.K. Prajapat, S.M. Sharma, A.K. Yusuf, G.P. Tyagi, Kothiyal, Mater. Sci. Eng. C **29**, 2226 (2009)
54. N.S. Gajbhiye, S. Bhattacharya, G. Balaji, R.S. Ningthoujam, R.K. Das, S. Basak, J. Weissmuller, Hyperfine Interact. **165**, 153 (2005)

Publisher's Note Springer Nature remains neutral with regard to jurisdictional claims in published maps and institutional affiliations.

Springer Nature or its licensor holds exclusive rights to this article under a publishing agreement with the author(s) or other rightsholder(s); author self-archiving of the accepted manuscript version of this article is solely governed by the terms of such publishing agreement and applicable law.